Alkalinity production coupled to pyrite formation represents an unaccounted blue carbon sink

Gloria M. S. Reithmaier[1], Scott G. Johnston[1], Tobias Junginger[2], Madeline M. Goddard[3], Christian J. Sanders[4], Lindsay B. Hutley[3], David T. Ho[5], Damien T. Maher[1,6]

[1]Southern Cross Geoscience, Southern Cross University, Lismore, New South Wales 2480, Australia

[2]Laboratory of Hydrology and Geochemistry, University of Strasbourg, 67000 Strasbourg, France

[3]Research Institute for the Environment and Livelihoods, Charles Darwin University, Darwin, Northern Territory 0810, Australia

[4]National Marine Science Centre, Southern Cross University, Coffs Harbour, New South Wales 2450, Australia

[5]Department of Oceanography, University of Hawaii at Manoa, Honolulu, Hawaii 96822, USA

[6]School of Environment, Science, and Engineering, Southern Cross University, Lismore, New South Wales 2480, Australia

Corresponding author: Gloria Reithmaier (g.reithmaier.10@student.scu.edu.au)

Key Points

- Alkalinity export from coastal vegetated habitats is a long-term carbon sink if alkalinity production is coupled to pyrite formation
- We present the first global model for pyrite stocks in mangroves, showing that mangrove pyrite stocks amount to, on average, 155 Mg/ha
- Pyrite formation in mangroves produces between 0.37 and 0.52 Tmol TAlk per year globally, making the process a substantial carbon sink

Abstract

Coastal vegetated habitats, including mangroves, saltmarshes and seagrasses, mitigate climate change by storing atmospheric carbon. Previous blue carbon research has mainly focused on organic carbon stocks. However, recent studies suggest that lateral inorganic carbon export might be equally important. Lateral export is a long-term carbon sink if carbon is exported as alkalinity (TAlk) produced via sulfate reduction coupled to pyrite formation. This study evaluates drivers of pyrite formation in coastal vegetated habitats, compares pyrite production to TAlk outwelling rates, and estimates global pyrite stocks in mangroves. We quantified pyrite stocks in mangroves, saltmarshes and seagrasses along a latitudinal gradient on the Australian East Coast, including a mangrove dieback area, and in the Everglades (Florida, USA). Our results indicate that pyrite stocks were driven by a combination of biomass, tidal amplitude, sediment organic carbon, sedimentation rates, rainfall latitude, temperature, and iron availability. Pyrite stocks were three-times higher in mangroves (103 ± 61 Mg/ha) than in saltmarshes (30 ± 30 Mg/ha) and seagrasses (32 ± 1 Mg/ha). Mangrove pyrite stocks were linearly correlated to TAlk export at sites where sulfate reduction was the dominant TAlk producing process, however pyrite generation could not explain all TAlk production. We present the first global model predicting pyrite stocks in mangroves, which average 155 (range 128 – 182) Mg/ha. In mangroves, estimated global TAlk production coupled to pyrite formation (~3 mol/m^2/y) is equal to ~24% of their global organic carbon burial rate, thus highlighting the importance of including TAlk export in future blue carbon budgets.

Plain Language Summary

Coastal vegetated habitats (i.e., mangroves, saltmarshes and seagrasses) buffer climate change by capturing carbon dioxide. The potential of these habitats to offset anthropogenic climate change is currently evaluated by measuring the amount of carbon that accumulates in coastal vegetated sediments. However, sedimentary carbon may be partly decomposed by microorganisms and can be exported to the coastal ocean. Exported carbon can be a permanent carbon sink if the carbon decomposition is coupled to the formation of iron sulfide minerals. This study explores the drivers and global relevance of iron sulfide mineral formation and the associated carbon export in coastal vegetated habitats. We found that biological, climatic and geological factors, can predict iron sulfide mineral formation. Based on these relationships, we developed the first global model predicting iron sulfide mineral stocks in mangroves and found that the associated dissolved carbon generated was equal to a quarter of the carbon stored in mangrove sediments. This highlights the importance of considering dissolved carbon export when evaluating the potential of coastal vegetated habitats to buffer climate change.

Keywords

Coastal carbon cycling
Mangrove carbon budget
Alkalinity generation
Sulfur cycling
Iron sulfide minerals
Chromium reducible sulfur

1 Introduction

Coastal vegetated habitats, such as mangroves, saltmarshes and seagrasses, mitigate climate change by sequestering and storing atmospheric carbon. Carbon sequestration and storage per unit area is considerably higher in coastal vegetated habitats compared to terrestrial ecosystems (Mcleod et al., 2011; Nellemann & Corcoran, 2009) and has been referred to "blue carbon". Previous blue carbon research focused mainly on sedimentary and biomass carbon stocks to evaluate the capacity of coastal vegetated habitats to mitigate climate change (Brown et al., 2016; Donato et al., 2011; Fourqurean et al., 2012; Kauffman & Bhomia, 2017; Kelleway et al., 2016). However, in addition to carbon stocks, dissolved carbon export is a significant, but so far largely unaccounted, blue carbon sink (Ho et al., 2017; Maher et al., 2018; Maher et al., 2013; Santos et al., 2019).

Dissolved carbon export from coastal vegetated habitats can be considered a long-term carbon sink if carbon is exported as alkalinity (TAlk), since exported TAlk has a residence time in the ocean of ~ 1 x 10^5 years (Emerson & Hedges, 2008; Middelburg et al., 2019). Flushing of porewater TAlk followed by lateral export to the coastal ocean is a major carbon sink in mangroves and saltmarshes (Sippo et al., 2016; Wang & Cai, 2004). Sedimentary processes that couple organic matter degradation and TAlk production include denitrification, manganese reduction, iron reduction and sulfate reduction (Burdige, 2011; Krumins et al., 2013). However, oxidation of reduced compounds (e.g. sulfide) may consume neo-formed TAlk prior to being exported. Therefore, only a permanent spatial decoupling of anaerobic remineralisation products from TAlk, such as loss via nitrogen gas from denitrification and precipitation of reduced sulfur as sedimentary pyrite, can contribute to net TAlk production (Hu & Cai, 2011). Due to nitrogen limitation, denitrification rates in pristine coastal vegetated habitats are usually low (Bianchi, 2007), and as such sulfate reduction coupled to pyrite formation is often the dominant net TAlk production process coupled to organic matter degradation in pristine coastal vegetated habitats.

In coastal sediments, pyrite (FeS_2) is formed via several, complex pathways. A common pathway involves iron(II) sulfide (FeS) as an initial precursor, which is formed from the reaction of sulfide, produced by microbially mediated sulfate reduction, with ferrous iron (Fe^{2+}) or with reactive iron(III) oxides (Schoonen & Barnes, 1991). Since sulfur in pyrite is slightly more oxidised (S-I) than in sulfide (S-II), pyrite is produced via intermediate redox reactions, including partial oxidation of FeS. Pyrite formation mainly occurs in upper sediment layers, where reactive iron concentrations and sulfate reduction rates are sufficiently high due to mixed redox conditions, adequate sulphate supply from surface waters, and available labile organic matter (Burdige, 2011; Wada & Seisuwan, 1986). Within this biogeochemically dynamic layer, pyrite can form via reaction of FeS with polysulfide (S_2^{x-}) or via a greigite intermediary (Fe_3S_4) (Goldhaber, 2003; Rickard & Luther, 2007). Alternatively, FeS can react with hydrogen sulfide to form pyrite and hydrogen gas (Rickard, 1997), especially within deeper sediment depths where sulfide concentrations are often comparatively high. Howarth (1979) observed that in saltmarshes, pyrite can also form rapidly without FeS as an initial precursor. In situ rates of pyrite formation depend on a wide range of environmental conditions (Burton et al., 2011).

The availability of sulfate, organic carbon and reactive iron are key factors controlling pyrite formation in coastal sediments (Berner, 1970, 1984). In coastal vegetated habitats, tidal seawater inundation resupplies the sulfate required for sulfate reduction. Therefore, sulfate is usually only limiting in upper estuarine freshwater reaches (where the salinity drops below 2.5 – 4), where sediments are impermeable, or in extremely carbon rich sediments (Burdige, 2011). Sulfate reduction also requires a source of organic carbon. Even though coastal

vegetated habitats are generally carbon rich, their carbon content is variable and depends on climatic factors, geomorphology, hydrology, vegetation species composition, nutrient availability and sedimentation rates (Kristensen et al., 2008; Macreadie et al., 2014; Ouyang & Lee, 2014; Sasmito et al., 2020). In carbon rich systems (>15% sediment organic carbon content), reactive iron availability can also limit pyrite formation (Berner & Raiswell, 1984). The availability of reactive iron depends on regional geology, sediment texture, weathering and sedimentation rates (Kendall et al., 2012; Raiswell & Canfield, 2012). Whether sulfate, organic carbon or reactive iron limits pyrite formation is highly site specific (Morse et al., 2007), hence modelling these processes is a challenge.

This study aims to evaluate alkalinity production coupled to pyrite formation in coastal vegetated habitats and to examine whether pyrite stocks represent a significant blue carbon sink. To achieve this, we quantified pyrite stocks in mangroves, saltmarshes and seagrasses along a latitudinal gradient. We also investigated relationships between pyrite stocks and key underlying drivers to develop a global model for mangrove pyrite stocks in order to provide a basis for estimating the pyrite-associated global mangrove TAlk generation. In order to investigate small-scale variability in pyrite stocks and consequences of vegetation disturbance on pyrite stocks, we conducted two case studies - one within a large, pristine mangrove system in Florida, USA and a second in a mangrove dieback area in Australia. We tested whether pyrite stocks can be used as a proxy for TAlk generation / export locally and hypothesise that pyrite stocks provide an important indirect means for estimating what is currently an uncounted blue carbon sink.

2 Methods

2.1 Study sites

We investigated pyrite stocks in three areas that span the general range of climatic, biomass, diversity, and sediment carbon stocks observed in mangroves globally, as well as covering a range in catchment geology (Figure 1, Table 1). Firstly, at Everglades National Park in Florida, USA, which contains the largest continuous mangrove forest in North America (144,447 ha), sampling was conducted along the Shark River estuary. The Shark River estuary is dominated by mangroves, with a transition to freshwater marsh areas in the freshwater reaches.

Secondly, we sampled an Australian mangrove dieback area located in the Gulf of Carpentaria near Karumba. During late 2015 and mid 2016 more than 7,400 ha of mangrove forest died as a result of high temperatures, drought and a rapid drop in sea levels during the pre-monsoon dry season (Duke et al., 2017; Lovelock et al., 2017). The Norman River separates a dead mangrove stand from an adjacent living mangrove area, allowing direct comparison to test the effect of the mangrove dieback on pyrite stocks in an identical climate zone.

Thirdly, we conducted sampling along a latitudinal gradient at the Australian East Coast (Figure 1, Table 1). Sampling areas along the latitudinal gradient from 12° to 38° included mangroves, saltmarshes and seagrasses located in Darwin, Hinchinbrook Island, Rockhampton, Seventeen Seventy, River Heads, Sunshine Coast, Jacobs Well, Ballina, Coffs Harbour, Queens Lake, Newcastle, Sydney and Barwon Heads.

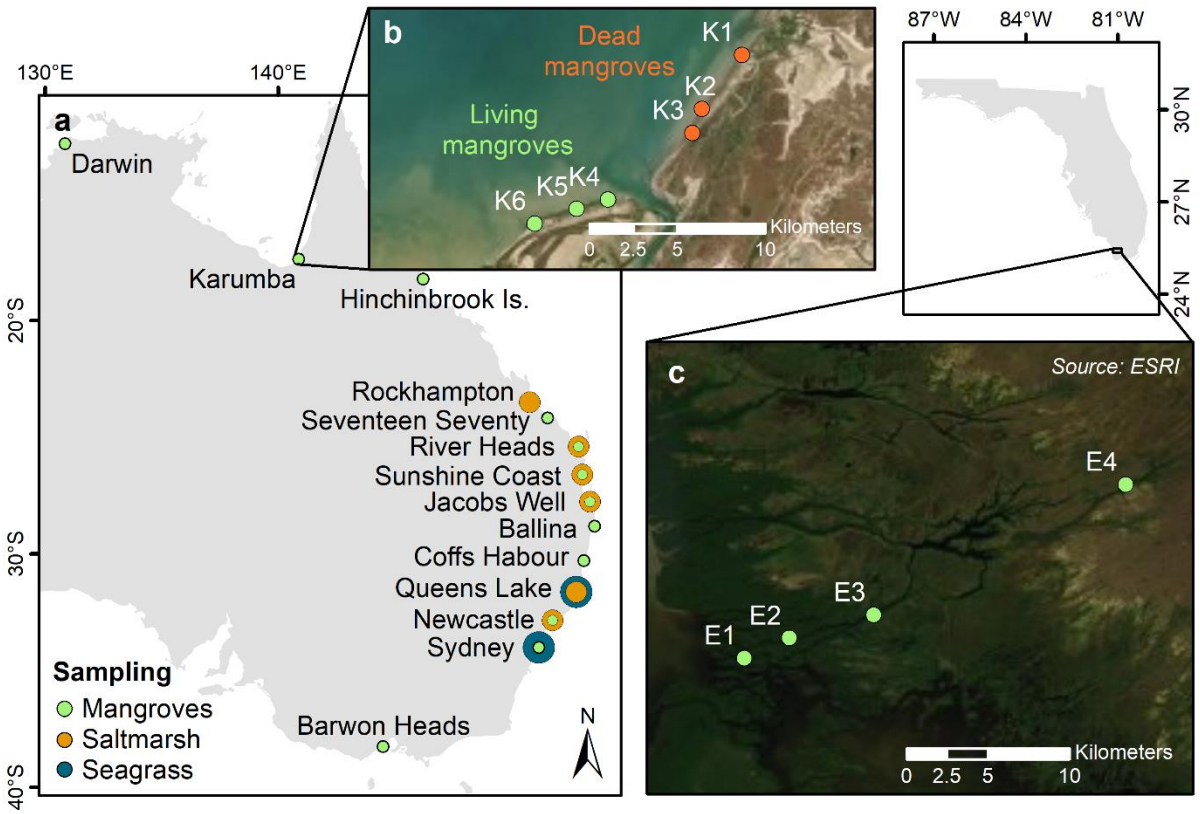

Figure 1. Study sites (a) along a latitudinal gradient at the Australian East Coast, (b) at the mangrove dieback area near Karumba and (c) along the Shark River estuary at the Everglades National Park, Florida, USA.

Table 1. Location, sampling dates and climate of all study sites. Annual temperature and rainfall were averaged between 1982 and 2012 (Climate-Data.org, 2020).

Site	GPS	Sample date (mm/yy)	Climate	Average annual temperature (°C)	Average annual rainfall (mm)
Everglades	25.36247°N, 81.0847°W	11/19	Subtropical	23.6	1534
Darwin	12.51966°S, 130.90603°E	08/14	Tropical	27.4	1694
Karumba	17.39480°S, 140.87355°E	08/18	Tropical	27.1	876
Hinchinbrook Island	18.24400°S, 146.22800°E	07/14	Tropical	24.2	2001
Rockhampton	23.50949°S, 150.78940°E	02/19	Subtropical	22.3	890
Seventeen Seventy	24.19202°S, 151.56975°E	07/14, 2/19	Subtropical	22.1	1196
River Heads	25.40981°S, 152.89394°E	02/19	Subtropical	21.6	1225
Sunshine Coast	26.61198°S, 153.05518°E	02/19	Subtropical	20.5	1788
Jacobs Well	27.78094°S, 153.37962°E	11/13, 2/19	Subtropical	19.9	1555
Ballina	28.82454°S, 153.57198°E	01/19	Subtropical	19.7	1805
Coffs Harbour	30.29447°S, 153.11755°E	04/20	Subtropical	18.8	1688
Queens Lake	31.63441°S, 152.79648°E	01/19	Subtropical	17.9	1579
Newcastle	32.85146°S, 151.76753°E	11/14, 1/19	Subtropical	18.0	1139
Sydney	34.00988°S, 151.19168°E	02/19	Subtropical	17.6	1309
Barwon Heads	38.25716°S, 144.48700°E	11/14	Temperate	14.8	666

2.2 Sample collection

At Everglades National Park in Florida, USA, two to three sediment cores were taken at four sites, between the estuary mouth and the freshwater reaches of the Shark River estuary. At each site, a core was collected adjacent to the river, ~5 m landward from the river, and ~10 m landward from the river. At Karumba, nine sediment cores were taken from the living and nine sediment cores were taken from the dead mangrove area, with triplicate cores taken in the lower, middle and upper stands (~75 m distance). At the sites along the Australian latitudinal gradient, one to three sediment cores were collected per ecosystem: 24 at mangrove, eleven at saltmarsh and four at seagrass sites. In mangrove and saltmarsh areas, sediment cores were taken from locations close to the low tide mark and at higher intertidal areas. In total 66 cores were collected from which 900 depth increments were analysed for pyrite. The maximum sampling depth varied between 33 cm and two meters, with most sediment cores (73%) having a depth of at least 90 cm.

Sediment cores were extracted with a Russian Peat auger or a gouge auger. The redox potential of the sediment profiles was measured with a handheld digital meter (Hach 40Qd). Samples for acid-volatile sulfide (AVS) and chromium-reducible sulfur (CRS) analysis, together known as reduced inorganic sulfur (RIS), were either subsampled on site into plastic bags with all air-removed, and kept frozen or subsampled from sediment cores, which were sealed with plastic shrink wrap, stored frozen and transported to the laboratory. Additional sediment samples were taken for dry bulk density, reactive iron and organic carbon measurements. At Darwin, Hinchinbrook Island, Seventeen Seventy, Jacobs Well, Newcastle, and Barwon Heads subsamples were taken to analyse sediment accumulation rates (SAR).

At selected Everglades and Karumba sites, porewater profiles were analysed for TAlk, Fe^{2+}, total aqueous iron (Fe^{Tot}) and aqueous sulfide (S(-II)), which includes H_2S, HS^- and S^{2-}. Porewater extraction was conducted as described by Johnston et al. (2016). Briefly, sediment cores were collected in PVC cores and 10 cm long rhizon samplers were inserted into the cores at increasing depths. Porewater was extracted under vacuum via tubing and Luer-Lock connectors through a needle into N_2 filled, O_2-free 10 ml glass vials, which were sealed with rubber septa. Porewater samples were analysed on the day of collection.

At Karumba, groundwater was sampled for TAlk analysis 1 m adjacent to the sediment core collection site. Boreholes were dug with a post-hole digger and purged three times with a peristaltic pump. Groundwater was allowed to completely recharge prior to sampling. Groundwater TAlk samples were stored cool and measured within one day.

2.3 Sample analysis

Sediment AVS, which includes intermediaries such as FeS and greigite, was analysed by the diffusion method outlined by Burton et al. (2009), extracting AVS with hydrochloric acid/ascorbic acid and trapping H_2S in an alkaline zinc solution. CRS was quantified sequentially after AVS analysis, using the method developed by Burton et al. (2008). Both AVS and CRS concentrations were determined via iodometric titration of the zinc traps, with a measurement error of 11% (based on repeat duplicate analysis) and a detection limit of 2 µmol/g.

Sediment organic carbon was analysed, as described by Radabaugh et al. (2018). In brief, the bulk density was determined by mass loss, drying the samples at 105 °C. Subsequently, organic carbon was determined by the loss-on-ignition (LOI) method, combusting samples at 550 °C. To convert LOI (%) into sediment organic carbon (%) an ecosystem specific conversation factor was used for mangroves (0.42), saltmarshes (0.50) and seagrasses (0.40) (Fourqurean et al., 2012; Radabaugh et al., 2018). In addition, for sediment cores taken in Darwin, Hinchinbrook Island, Seventeen Seventy, Jacob's Well, Newcastle and Barwon Heads, organic carbon was analysed using a Flash Elemental Analyzer coupled to a Thermo Fisher Delta V isotope ratio mass spectrometer.

Reactive iron was estimated using the citrate-dithionite extraction method, which extracts the most reactive iron(III) oxide phases and represents a pool of readily "available" Fe that can contribute to pyrite formation (Raiswell et al., 1994; Raiswell & Canfield, 2012). After filtration (0.45 µm), reactive iron was measured by spectrophotometry using the 1,10-phenanthroline method (APHA, 2005).

Porewater Fe^{2+}, Fe^{Tot} and S(-II) were also measured by spectrophotometry. The 1,10-phenanthroline method was used to determine porewater Fe^{2+} and, after reducing Fe^{3+} by adding hydroxylamine, Fe^{Tot} (APHA, 2005). Aqueous S(-II) was analysed using the methylene blue method (Cline, 1969).

Groundwater TAlk was determined by a Gran titration using a titrator (Metrohm 888 Titrando with Tiamo light) with a precision better than 5 µM. Drifts and deviations in the acid concentration were corrected using certified reference materials (CRM batch 175 and CRM batch 178), as described by Dickson (2010).

SAR was determined examining the nuclear fallout signature of plutonium-239 + 240 as described by Sanders et al. (2016b) with an uncertainty of 16%. In brief, samples were dry-ashed, spiked with Pu-242 and filtered (0.45 µm). To allow conversion from Pu to Pu(IV)

samples were standing open for 16 hours. Analysis was performed using a Thermo X2 Series quadrupole ICPMS system.

2.4 Calculations and statistics

Pyrite concentrations were calculated by dividing CRS concentrations by two, assuming that the stoichiometry of pyrite is FeS_2 and that elemental sulfur, which may contribute to CRS, is negligible. These assumptions are reasonable since elemental sulfur is often negligible in coastal vegetated habitats and thus FeS_2 is the dominant form of CRS (Ding et al., 2014; Holmer et al., 2006; Johnston et al., 2016). Pyrite and carbon stocks were calculated by summing the pyrite and sediment organic carbon density (concentrations multiplied by the dry bulk density) over the first meter of each sediment core. If cores were shorter than 1 m, the deepest measured pyrite concentration and bulk densities were extrapolated to 1 m.

The degree of pyritisation (DOP), a proxy for iron limitation, was calculated according to Berner (1970):

$$\text{DOP} = \text{pyrite iron} / (\text{pyrite iron} + \text{reactive iron}), \text{ where pyrite iron} = 0.5 \times \text{CRS} \quad (1)$$

At sites where SAR was determined, TAlk production rates coupled to pyrite formation, as well as carbon burial rates were estimated. Mass accumulation rates (MAR) were calculated as the product of SAR and dry bulk density. Multiplying MAR with the carbon concentration at each depth, carbon accumulation rates were calculated and averaged per core. Similarly, pyrite accumulation rates were calculated by multiplying pyrite concentrations with MAR per depth and averaged per core. The TAlk production during pyrite formation is coupled to the stoichiometry of sulfate reduction. During sulfate reduction, approximately 2 - 3 TAlk equivalents are produced per mol of reduced sulfate (SO_4^{2-}), with the ratio depending on the organic substrate, i.e., acetate (CH_3COO^-), lactate ($3CH_3CHOHCOO^-$) or propionate ($CH_3CH_2COO^-$) (Sheoran et al., 2010):

$$CH_3COO^- + SO_4^{2-} + H^+ \rightarrow H_2S + 2HCO_3^- \quad (2)$$

$$2/3CH_3CHOHCOO^- + SO_4^{2-} + 2/3H^+ \rightarrow H_2S + 2HCO_3^- \quad (3)$$

$$4/7CH_3CH_2COO^- + SO_4^{2-} + 6/7H^+ \rightarrow H_2S + 12/7HCO_3^- \quad (4)$$

Given that 2 mols of reduced sulfur are required for a single mol of pyrite (Blodau, 2006; Johnston et al., 2012), pyrite accumulation rates were multiplied by a conversion factor of 5 to estimate TAlk production rates coupled to pyrite formation. Uncertainty bands were estimated by propagating the error related to the conversion factor (±1) as well as the measurement errors of the pyrite (± 11%) and SAR (± 16%) analysis.

Statistical analysis was conducted in R-3.6.2. Probability levels for are indicated as * if $p < 0.05$, ** if $p < 0.01$ and *** if $p < 0$ .001. A log-linear model based on site-specific average annual temperature, average annual precipitation, average tidal amplitude, sediment organic carbon, aboveground biomass, and reactive iron in the catchment was developed to predict mangrove pyrite stocks. Constants were calculated through an iterative least-squares process using Microsoft Excel. The resulting model output was used to estimate global pyrite stocks in mangroves. The global model inputs included temperature (Fick & Hijmans, 2017), precipitation (Fick & Hijmans, 2017), average tidal amplitude (Vestbo et al., 2018), sediment organic carbon (Sanderman et al., 2018), aboveground biomass (Simard et al., 2019), and reactive iron (Rossel et al., 2016). We conducted Monte Carlo error simulations to calculate

the 25% and 75% quartile error band of the global pyrite stock average by taking the RMSE of the model and running 1,000,000 simulations.

3 Results

3.1 Everglades National Park

At Everglades National Park, bulk density ranged between 0.09 and 0.94 g/cm^3 and AVS was below the detection limit in all samples. Pyrite concentrations (3.4 – 408 µmol/g) were higher at the polyhaline downstream (E1) and mesohaline midstream (E2, E3) sites compared to the oligohaline upstream site (E4) and generally increased with depth (Figure 2). There was no significant difference in the pyrite concentrations with increasing distance from the river.

On average, porewater Fe^{Tot} (0.62 – 25 µM) was two-times higher at the upstream site (E4) compared to the mid and downstream sites (E1, E3) and decreased with depth. The share of porewater Fe^{2+} (0.17 – 6.8 µM) on Fe^{Tot} increased with depth and was highest at the midstream and downstream sites (up to 100% at E1 and E3). Increasing with depth, porewater TAlk (1345 – 14840 µmol/kg) was two-times higher at the downstream and midstream sites (E1 and E3) compared to the upstream site (E4).

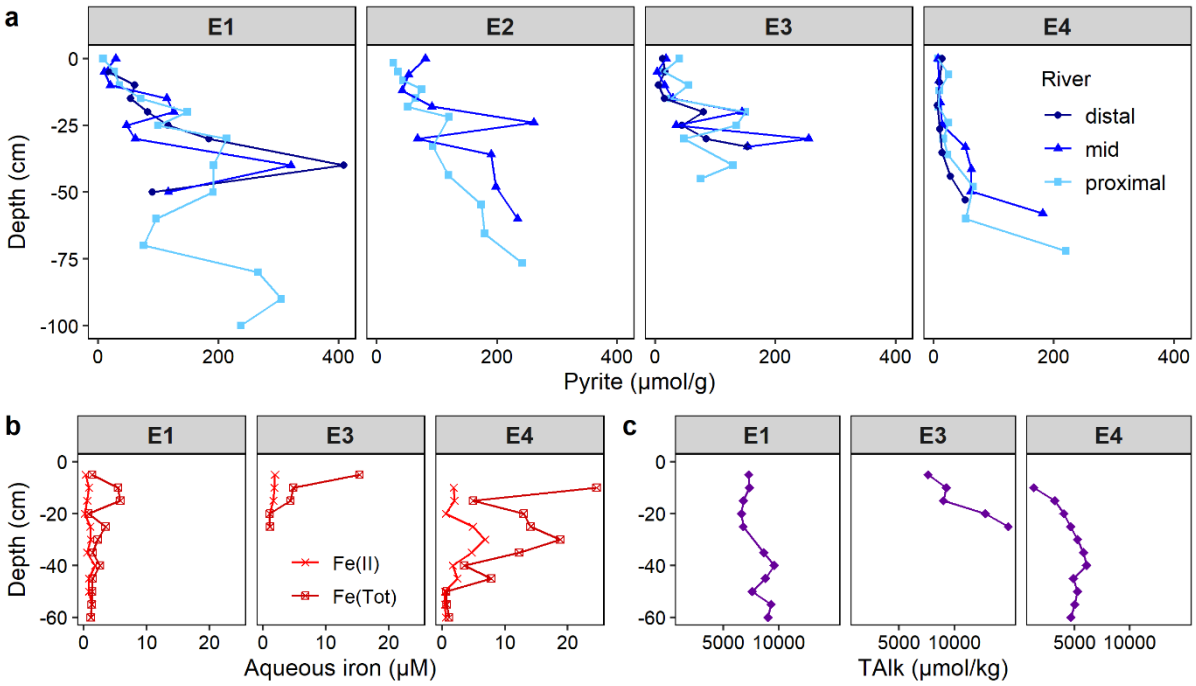

Figure 2. Sediment profiles of (a) pyrite, (b) porewater iron, and (c) porewater alkalinity concentrations at downstream (E1), midstream (E2, E3), and upstream (E4) sites along the Shark River estuary at Everglades National Park, Florida, USA. At each site, cores were taken at an increasing distance from the river (~5m).

3.2 Mangrove dieback near Karumba

At the Karumba mangrove site, the bulk density varied between 0.37 and 1.7 g/cm^3. Concentrations of AVS ranged from 0 to 5.3 µmol/g and were below the detection limit in the majority of the samples. Pyrite reached higher values (0 – 217 µmol/g) at the living (K4 – K6) than at the dead mangrove area (0 – 127 µmol/g, K1 – K3) (Figure 3). Pyrite concentrations decreased with distance from the shore, however, this effect decreased with depth, particularly at the dead area. The redox potential indicated anoxic conditions at close proximity to the ocean (-321 to -109 mV), but partly suboxic conditions at mid (-215 to 12 mV) and distal (-145 to 231 mV) cores.

Decreasing with depth, reactive iron was on average two times lower at the living (0.25%) than at the dead (0.41%) area. The DOP was almost twice as high at the living (0.72) than at the dead (0.43) area. Porewater Fe^{2+} ranged from 1 – 57 µM. At the living area, Fe^{2+} accounted for an average of 24% of Fe^{Tot} (1.6 – 83 µM), which showed two distinct peaks at 20 and 40 cm. At both areas, porewater S(-II) (0.11 – 8543 µM) and TAlk (1400 – 52000 µmol/kg) increased simultaneously with depth. At the living area, S(-II) increased abruptly just below the lower Fe^{Tot} peak.

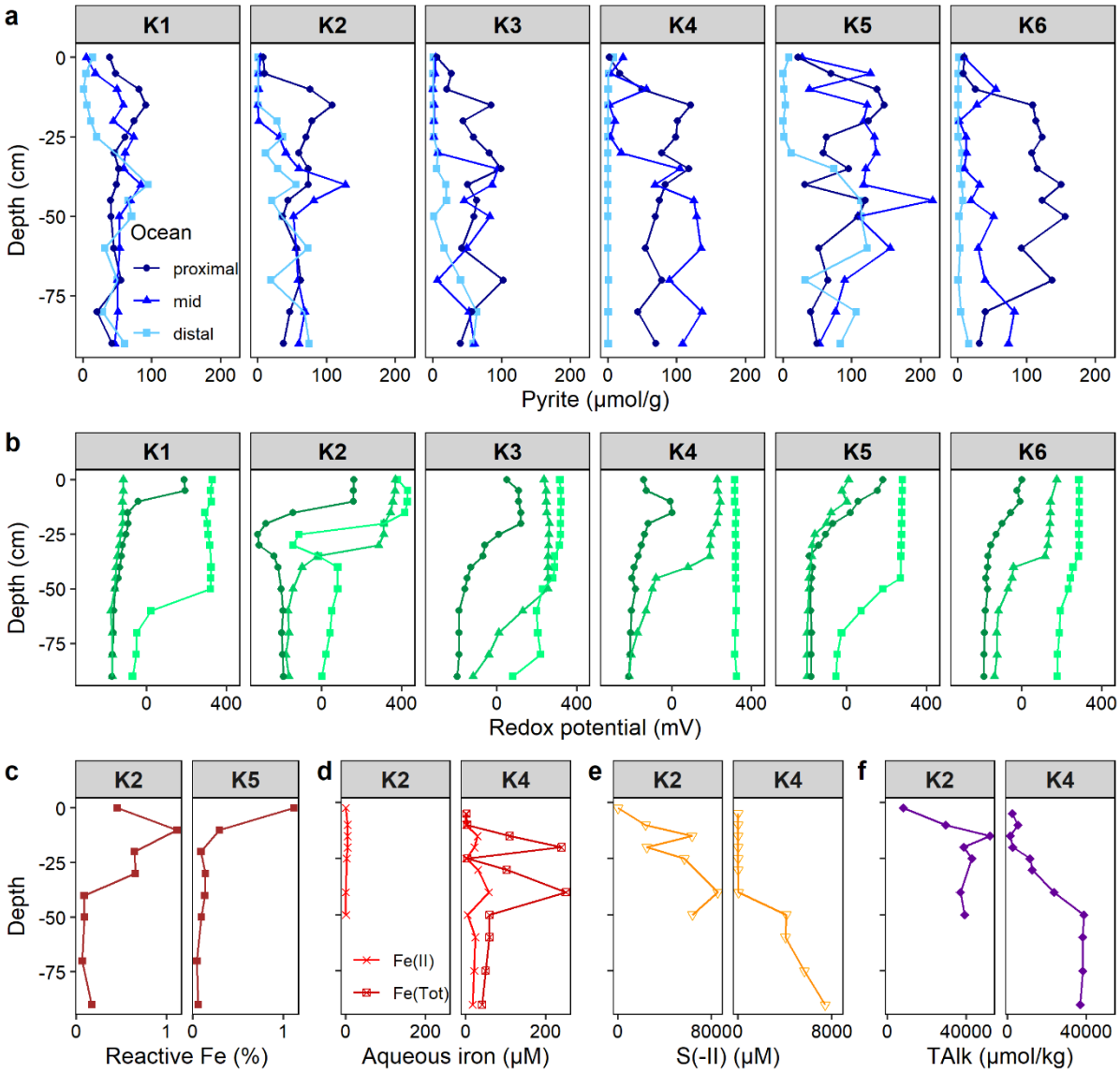

Figure 3. Sediment profiles of (a) pyrite, (b) redox potential, (c) reactive iron, (d) porewater iron, (e) porewater S(-II) and (f) porewater alkalinity at dead mangrove areas (K1 – 3) and living mangrove areas (K4 – 6) near Karumba, Australia. At each site, cores were taken at an increasing distance from the ocean (~75m).

On average, pyrite stocks were 20% lower at the dead (range 21 – 74 Mg/ha, mean ± error 50 ± 15 Mg/ha) compared to the living area (1 – 124 Mg/ha, 63 ± 40 Mg/ha) (Figure 4). Pyrite stocks were positively correlated with groundwater TAlk (ranging from 7400 to 48000 µmol/kg) in the living area, (R^2 = 0.59*), but showed no significant correlation at the dead area.

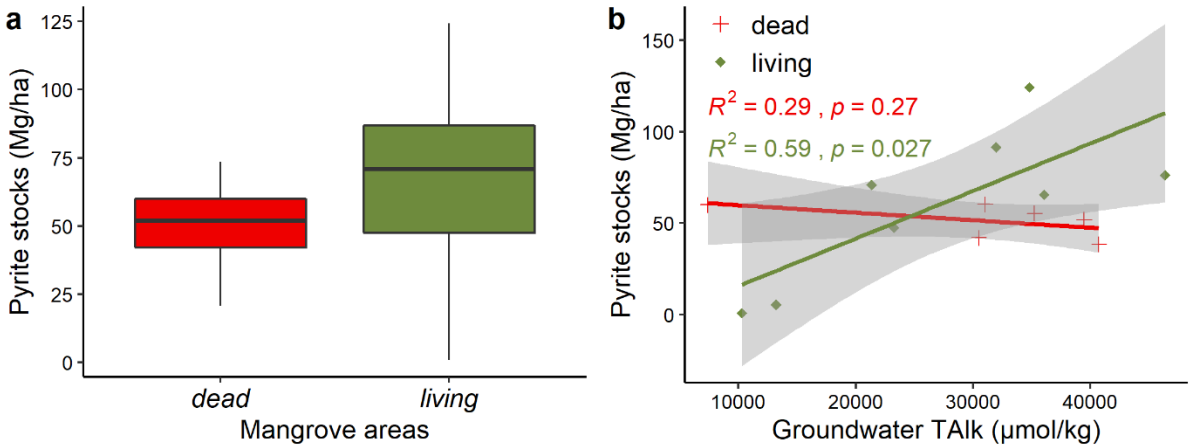

Figure 4. Comparison of (a) pyrite stocks and (b) correlations between pyrite stocks and groundwater TAlk at the dead (n = 9) and living (n = 9) mangrove areas near Karumba, Australia. Grey areas indicate the 95% confidence intervals of the regressions.

3.3 Latitudinal gradient

Along the latitudinal gradient at the Australian East Coast, AVS concentrations in mangrove sediments spanned 0 – 37 µmol/g (3.2 ± 5.7 µmol/g), accounting for an average of only 2% of RIS. Consequently, CRS was the dominant form (98%) of RIS. Compiling the entire dataset (excluding dead mangrove area), pyrite reached highest values in mangroves (0 – 645 µmol/g, 0 – 7.7%), followed by saltmarshes (0 – 395 µmol/g, 0 – 4.7%) and seagrasses (2.5 – 59 µmol/g, 0.03 – 0.71%) (Figure 5).

In mangrove and saltmarsh sediments, pyrite increased with depth, whereas in seagrass sediments, pyrite marginally decreased with depth (Figure 5). Furthermore, pyrite correlated with sediment organic carbon in mangroves (0.16 – 19%, R^2 = 0.24***), but not in saltmarshes (0.43 – 8.6%, R^2 = 0.001) or seagrasses (0.021 – 1.6%, R^2 = 0.09). Reactive iron reached the highest levels in mangroves (0 – 4.2%), followed by saltmarshes (0 – 2.9%) and seagrasses (0.1 – 1.0%), and was negatively correlated with pyrite in mangroves (R^2 = 0.17***). The redox potential in mangrove (-216 to 438 mV), saltmarsh (-48 to 364 mV), and seagrass (-30 to 207 mV) sediments showed no significant correlation with pyrite (data not shown).

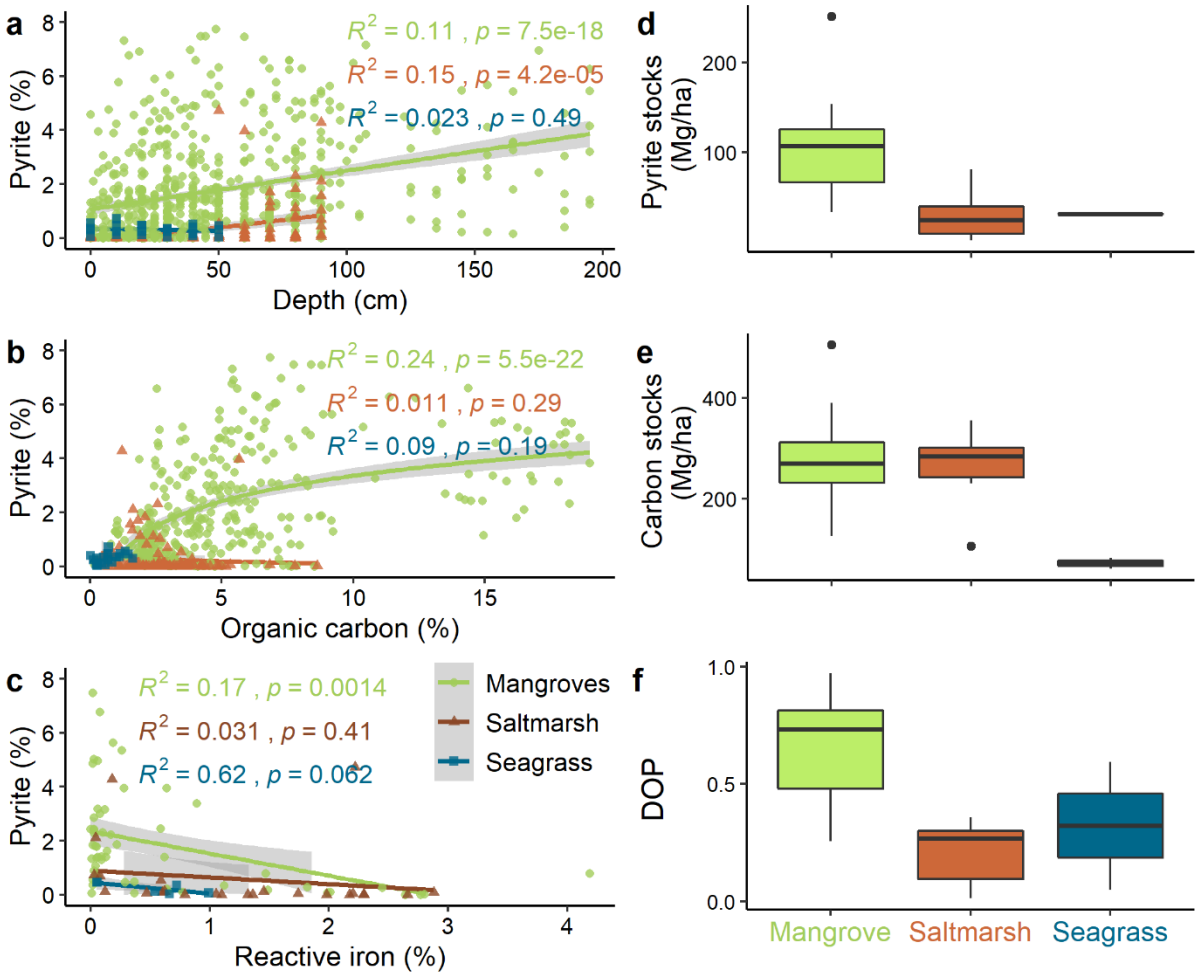

Figure 5. Relationship between pyrite and (a) depth, (b) sediment carbon and (c) reactive iron. Boxplots of (d) pyrite stocks, (e) sediment carbon stocks and (f) degree of pyritization at mangrove (n = 14), saltmarsh (n = 6) and seagrass (n = 2) sites. Stocks are calculated for 1 m depth. Grey areas indicate the 95% confidence intervals of the regressions.

Pyrite stocks were three-times higher in mangroves (103 ± 61 Mg/ha) than in saltmarshes (30 ± 30 Mg/ha) and seagrass (32 ± 1 Mg/ha) sites (Figure 5, Table 2). In saltmarshes, pyrite stocks were on average, threefold higher in cores taken closer to the water edge compared to cores taken at a higher elevation in the tidal frame, whereas at mangroves no difference was found. Carbon stocks, calculated for 1 m depth, in mangroves (249 ± 58 Mg/ha) and saltmarshes (261 ± 86 Mg/ha), were three-times higher than in seagrasses (72 ± 15 Mg/ha). On average, carbon stocks were two-times higher than pyrite stocks at mangroves and seagrasses, and nine-times higher at saltmarshes. The DOP was considerably higher at mangroves (0.7 ± 0.2) than at saltmarshes (0.2 ± 0.1) and seagrasses (0.3 ± 0.4).

328 **Table 2.** Average pyrite stocks, sediment carbon stocks and degree of pyritisation (DOP) for 1 m depth at mangrove, saltmarsh and seagrass sites.

Site	Pyrite stock (Mg/ha)			Sediment carbon stocks (Mg/ha)			DOP (%)		
	Mangrove	**Saltmarsh**	**Seagrass**	**Mangrove**	**Saltmarsh**	**Seagrass**	**Mangrove**	**Saltmarsh**	**Seagrass**
Everglades	56						0.74		
Darwin	252			283			0.92		
Karumba	63 ± 40						0.72		
Hinchinbrook Island	113			364			0.97		
Rockhampton		2 ± 2			304 ± 10			0.01	
1770	92 ± 11			194 ± 12			0.73		
River Heads	67 ± 1	82 ± 97		223 ± 16	293 ± 16		0.26	0.36	
Sunshine Coast	107 ± 50	25 ± 25		270 ± 19	276 ± 27		0.61	0.26	
Jacobs Well	126 ± 24	45 ± 18		216 ± 56	231 ± 18		0.75	0.28	
Ballina	154 ± 52			308 ± 24			0.48		
Coffs Harbour	142 ± 7			317			0.81		
Queens Lake		24	31 ± 28		106	61 ± 4		0.31	0.05
Newcastle	122 ± 24	4 ± 3		220 ± 50	356 ± 121		0.43	0.04	
Sydney	34 ± 1		33 ± 13	182 ± 23		83 ± 5	0.85		0.59
Barwon Heads	93			204			0.36		
Average	109 ± 55	30 ± 30	32 ± 1	253 ± 59	261 ± 86	72 ± 15	0.7 ± 0.2	0.2 ± 0.1	0.3 ± 0.4

Drivers of mangrove pyrite stocks were investigated (Table 3). Pyrite stocks were positively correlated with aboveground biomass (r = 0.62*), average annual tidal amplitude, sediment carbon stocks (r = 0.50), sedimentation rates (r = 0.47), average annual rainfall (r = 0.45), latitude (r = -0.41), average annual temperature average (r = 0.25), and reactive iron within the catchment (r = 0.24). Pyrite stocks were not correlated with average surface water salinities.

Table 3. Explanatory variables and Pearson correlations with pyrite stocks, variables that were used as model data inputs. Annual temperature and rainfall were averaged between 1982 and 2012 (Climate-Data.org, 2020). Average annual tidal amplitude was retrieved from Bureau of Meteorology (2020). Reactive iron was averaged for a 50 km radius around the sites (Rossel et al., 2016).

Site	Latitude	Av. annual temperature (°C)	Av. annual rainfall (mm)	Av. annual tidal amplitude (m)	Average salinity	Sediment carbon stocks (MgC/ha)	Aboveground biomass (MgC/ha)	Reactive iron (mg/g)	Sedimentation rate (cm/y)
Everglades	25	23.6	1534	0.9	27[a]	366[g]	71[g]	1	0.36[m]
Darwin	-12	27.4	1694	7.1	35[b]	391[h]	113[h]	5	0.63
Karumba	-17	27.1	876	3.5		123[i]	29[i]	9	0.77[i]
Hinchinbrook I.	-18	24.2	2001	3.3	35[b]	506[h]	73[h]	3	0.51
Seventeen Seventy	-24	22.1	1196	4.2	37[b]	241[h]	41[h]	4	0.13
River Heads	-25	21.6	1225	3.1		223	35	5	
Sunshine Coast	-26	20.5	1788	2.0	15[c]	270	46[j]	8	
Jacobs Well	-27	19.9	1555	1.8	37[b]	272[h]	35[h]	5	0.27
Ballina	-28	19.7	1805	1.7	30[d]	308	48[j]	9	0.78[n]
Coffs Harbour	-30	18.8	1688	1.7	15[e]	317	52[j]	27	0.51[m]
Newcastle	-32	18.0	1139	1.8	33[b]	257[h]	32[h]	7	0.20
Sydney	-34	17.6	1309	1.8	35[f]	182	36[j]	4	0.04[n]
Barwon Heads	-38	14.8	666	1.2	35[b]	271[h]	2[h]	10	0.27

[a]Reithmaier et al. (2020); [b]Sippo et al. (2016); [c]Brown et al. (2018); [d]Maher et al. (2015); [e]Jeffrey et al. (2018); [f]Lee and Patterson (2002); [g]Jerath et al. (2016); [h]Sanders et al. (2016a); [i]Sippo et al. (2020); [j]Simard et al. (2019); [k]Smoak et al. (2013);[l]Logan et al. (2011); [m]Conrad et al. (2017); [n]Macreadie et al. (2012)

Along the latitudinal gradient, average SAR ranged from 0.13 – 0.63 cm/y and MAR from 0.08 – 0.27 g/cm^2/y (Table 4). Pyrite accumulation and resulting TAlk production were lowest at temperate Barwon Heads (0.04 mmol/m^2/d and 0.2 ± 0.05 mmol/m^2/d, respectively) and highest at tropical Darwin (0.41 mmol/m^2/y and 16 ± 4 mmol/m^2/d, respectively), which showed highest MAR and pyrite concentrations. TAlk production coupled to pyrite formation is equal to 1 – 41% of the carbon burial rates, which ranged between 7 and 39 mmol/m^2/d.

Table 4. Parameters required to estimate TAlk generation associated with pyrite formation and carbon burial rates. Values SAR and carbon burial rates were retrieved from Smoak et al. (2013).

Site	SAR (cm/y)	MAR (g/cm^2/y)	Pyrite accumulation (mmol/m^2/d)	Estimated TAlk production (mmol/m^2/d)	Carbon burial (mmol/m^2/d)
Everglades	0.36	0.12	0.41	2 ± 0.6	34
Darwin	0.63	0.27	3.27	16 ± 4	39
Seventeen Seventy	0.13	0.08	0.23	1 ± 1.4	9
Hinchinbrook Island	0.51	0.13	1.08	5 ± 0.3	48
Jacobs Well	0.27	0.16	0.88	4 ± 1.1	21
Newcastle	0.20	0.15	0.22	1 ± 0.3	7
Barwon Heads	0.27	0.14	0.04	0.2 ± 0.05	14

4 Discussion

4.1 Pyrite formation in coastal vegetated habitats

Sulfate reduction rates and reactive iron availability are the key drivers impacting the pyrite formation and thus the development of pyrite stocks (Berner, 1984, Figure 6). Seagrasses typically inhabit subtidal environments, where sulfate from overlying seawater is transported into their sediments via porewater diffusion and bioturbation (Chanton et al., 1987), which can limit sulfate availability and thus pyrite formation in deeper sediments. In mangroves and saltmarshes, sulfate is resupplied during each flood tide, whereby tidal pumping drives effective porewater exchange, encouraging flushing of TAlk and transporting sulfate into deeper sediment layers, facilitating sulfate reduction (Hemond et al., 1984; Sadat-Noori et al., 2017). These differences in hydrodynamics and sulfate supply likely contribute to the significantly higher pyrite concentrations observed in mangroves and saltmarshes, when compared to seagrasses in our study. At the mangrove sites, average surface water salinities were well above the level (>15) at which sulfate availability can limit sulfate reduction (2.5 – 4) (Burdige, 2011), suggesting that sulfate availability was not a limiting factor for pyrite formation at our study sites.

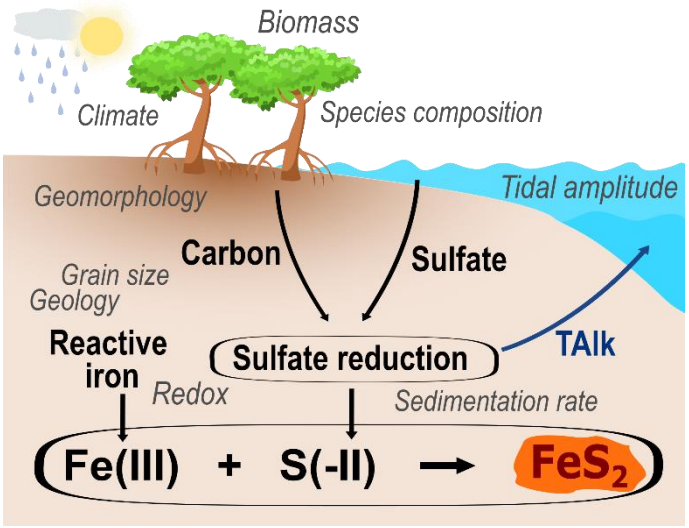

Figure 6. Direct (bold, black) and indirect (italic, grey) drivers of pyrite formation in coastal vegetated habitats.

In addition to sulfate supply, sulfate reduction requires organic carbon loading in excess of the aerobic respiration capacity. Coastal vegetated habitats store a large amount of organic carbon in their sediments (Mcleod et al., 2011), typically fuelling high sulfate reduction rates. Berner and Raiswell (1984) stated that usually only in extremely carbon-rich systems (>15%), factors other than organic carbon, e.g., reactive iron, limit pyrite formation. In our study, sediment organic carbon exceeded 15% only at mangroves on Hinchinbrook Island, whereas at most sites sediment organic carbon was below 10%, thus suggesting that organic carbon might be a major factor controlling pyrite formation at coastal vegetated habitats. Accordingly, pyrite was significantly correlated with sediment organic carbon in both mangroves and seagrasses, underlining the importance of organic carbon on pyrite formation in these systems. Similarly, previous mangrove studies found correlations between organic carbon and pyrite (Crémière et al., 2017; Ding et al., 2014; Ferreira et al., 2007b; Sherman et al., 1998). The positive correlation between mangrove pyrite stocks and SAR suggests that high SAR may limit the degradation of organic matter via aerobic carbon mineralisation pathways (Berner, 1984; Raiswell & Canfield, 2012), thus providing labile

carbon for sulfate reduction. At the seagrass sites, sediment carbon stocks were three times lower than that at mangroves and saltmarshes, which may contribute to the comparatively low pyrite stocks in seagrasses. Sediment organic carbon and pyrite concentrations showed no significant correlation at saltmarsh sites, suggesting that other limiting factors, such as less favourable redox conditions, might be more relevant controls on pyrite formation at the saltmarsh sites.

In addition to sedimentary organic carbon, vegetation itself can impact pyrite formation. Mangrove pyrite stocks were significantly correlated with aboveground biomass (r = 0.65*). Biomass might be a more conservative proxy for carbon availability than sediment carbon stocks, which are highly heterogenous (Brown et al., 2016). Furthermore, aboveground biomass can be regarded as a proxy for belowground biomass (Komiyama et al., 2008), which actively influences pyrite formation. Roots may facilitate pyrite formation by lowering the pH, releasing exudates, stimulating sulfate reducing bacteria and creating local oxidising conditions required for partial FeS oxidation (Ferreira et al., 2007a; Giblin, 1988; Holmer et al., 1994; Holmer et al., 2006; Morse, 1999). Previous studies have found higher pyrite content in vegetated habitats than adjacent unvegetated sediments, highlighting the importance of vegetation on pyrite formation (Andrade et al., 2012; Ferreira et al., 2007a; Giblin, 1988; Holmer et al., 2003; Otero et al., 2009). The degree to which the vegetation impacts pyrite formation varies between species, depending on root characteristics and primary productivity (Holmer et al., 2006; Sherman et al., 1998).

In addition to sulfate reduction rates, reactive iron is a critical ingredient for pyrite formation. Previous studies observed that reactive iron availability impacted pyrite formation in mangroves (Ferreira et al., 2007b; Otero et al., 2009), saltmarshes (Giblin, 1988; Morse et al., 2007) and seagrasses (Holmer et al., 2003; Morse, 1999), which were characterised by a sandy sediment texture or calcareous sediments and were thus iron-poor. Reactive iron was negatively correlated with pyrite at all coastal vegetated habitats. This can be explained by the biogeochemical zonation of coastal sediments (Froelich et al., 1979; Johnston et al., 2011). Pyrite and S(-II) increased with depth, whereas reactive iron(III) oxides are consumed and Fe^{2+} decreased under more reducing conditions associated with pyrite formation. The DOP is a more effective measure to evaluate the effect of reactive iron on pyrite formation than in situ iron concentrations. The DOP was considerably higher at mangroves (up to 0.97) than at saltmarsh (up to 0.36) and seagrass (up to 0.59) sites, suggesting that only at some mangrove sites pyrite formation was limited by reactive iron. At Hinchinbrook Island (DOP = 0.97) and Darwin (DOP = 0.92), sites that were characterised by high sediment organic carbons stocks, DOP was particularly high, thus suggesting iron limitation. Furthermore, mangrove pyrite stocks showed a positive correlation with average reactive iron within a 50 km radius around the sites, suggesting that the catchment geology also impacted pyrite formation.

Sedimentary pyrite accumulation requires mixed redox conditions for the formation of polysulfides or the partial oxidation of FeS (Luther III et al., 1982). In coastal vegetated habitats, roots and bioturbation can create oxidised microzones promoting pyrite formation. However, intense bioturbation and high rates of primary production (and oxygen release from roots) can also lead to oxidation of pyrite (Ferreira et al., 2007a; Giblin, 1988; Holmer et al., 1994; Holmer et al., 2006; Luther III et al., 1982). In intertidal mangroves and saltmarshes, redox conditions are strongly moderated by the water level. Consequently, pyrite formation can vary considerably between different geomorphological settings and locations within an ecosystem (Ferreira et al., 2007b; Giblin, 1988; Machado et al., 2014; Sherman et al., 1998). At Karumba, pyrite decreased slightly with increasing distance to the ocean, which was

accompanied by an increasing redox potential. However, the proximity to the water edge (i.e. tidal channel) did not generally affect measured mangrove pyrite stocks. In contrast, saltmarsh pyrite stocks decreased noticeably with increasing distance from the water edge. The fact that saltmarsh pyrite stocks were threefold lower than mangrove pyrite stocks, despite equal carbon stocks and lower DOP, is likely due to more oxidising conditions in the upper sediment layers, since saltmarshes occupy spaces higher in the tidal frame than mangroves and have therefore a shorter hydroperiod. This is supported by the change in pyrite concentrations going down core in saltmarshes, where pyrite was close to zero in the upper sediment layers and increased abruptly after around 40 – 80 cm (Figure 5).

Climatological and physical factors indirectly influence pyrite formation via their impacts on sulfate reduction and reactive iron availability. For example, mangrove pyrite stocks were significantly correlated with the tidal amplitude (r = 0.57*). Higher tidal amplitude increases porewater exchange (Tait et al., 2016), thereby resupplying sulfate, removing aqueous reaction products and transporting allochthonous organic carbon and reactive iron through the sediments. Furthermore, mangrove pyrite stocks were also positively correlated with average annual temperature and rainfall, which affect sedimentary organic carbon and aboveground biomass (Hutchison et al., 2014; Sanders et al., 2016a). Moreover, microbial sulfate reduction is highly temperature dependant (Robador et al., 2016; Westrich & Berner, 1988). Increasing rainfall drives weathering rates and sediment transport, and thus influences reactive iron supply from surrounding catchments (Kendall et al., 2012).

4.2 Mangrove pyrite formation represents an overlooked blue carbon sink

The blue carbon paradigm has focused primarily on the role of coastal vegetated ecosystems being hotspots of organic carbon burial and subsequently large sedimentary carbon stocks, whereas TAlk production has been largely overlooked (Maher et al., 2018). During sulfate reduction, organic carbon is converted into bicarbonate ions, some of which are exported from mangroves to the ocean via tidal porewater exchange (Krumins et al., 2013; Sippo et al., 2016), whereas sedimentary pyrite is sequestered *in situ*. This spatial decoupling of two key products of sulfate reduction (pyrite and bicarbonate ions) leads to a net generation of TAlk and generates a long-term carbon sink in the form of marine bicarbonate. As such, we argue that the blue carbon framework should incorporate a more holistic biogeochemical perspective which encompasses not only in situ sedimentary organic carbon sequestration, but also pyrite formation and its attendant TAlk export. This is supported by our results that show TAlk production associated with pyrite formation can account for up to 42% of the organic carbon burial rate and represents therefore a quantitatively relevant carbon sink.

At the Everglades and Karumba, porewater TAlk increased simultaneously with S(-II) and pyrite, highlighting the importance of pyrite formation for TAlk production. Sherman et al. (1998) also observed a significant correlation between pyrite and TAlk in mangrove sediments, but the correlation was restricted to deeper sediments, suggesting that TAlk in surface sediments was either exported by tidal flushing or driven by other processes. At the Everglades National Park and at mangrove sites near Karumba, porewater TAlk was on average six-times higher than average TAlk of seawater (2300 µmol/kg; Millero et al., 1998), indicating that mangrove sediments can act as a TAlk source to coastal waters, since tidal pumping drives effective porewater exchange (Tait et al., 2016).

We calculated the TAlk production coupled to pyrite formation and compared it to published lateral TAlk export rates (Figure 7). A significant linear correlation was found for Barwon Heads, Jacobs Well, Hinchinbrook Island and Darwin. In contrast, Newcastle,

Seventeen Seventy and the Everglades had disproportionally high TAlk export rates despite apparently low TAlk production coupled to pyrite formation. The high TAlk export rates might be due to a range of alternative TAlk producing processes. For example, at the Everglades, mangroves populate a large carbonate platform and therefore carbonate dissolution contributes substantially to TAlk production (Ho et al., 2017). At Newcastle, high denitrification rates caused by high nutrient freshwater inputs (Maher et al., 2016) may decouple lateral TAlk export and pyrite formation. Being located in the dry tropics, Seventeen Seventy had the lowest carbon stocks and slowest SAR, which might have favoured other carbon decomposition processes over sulfate reduction. Overall, our results and analysis suggest that pyrite formation is only a robust proxy for total TAlk production and export if sulfate reduction is the dominant TAlk producing process.

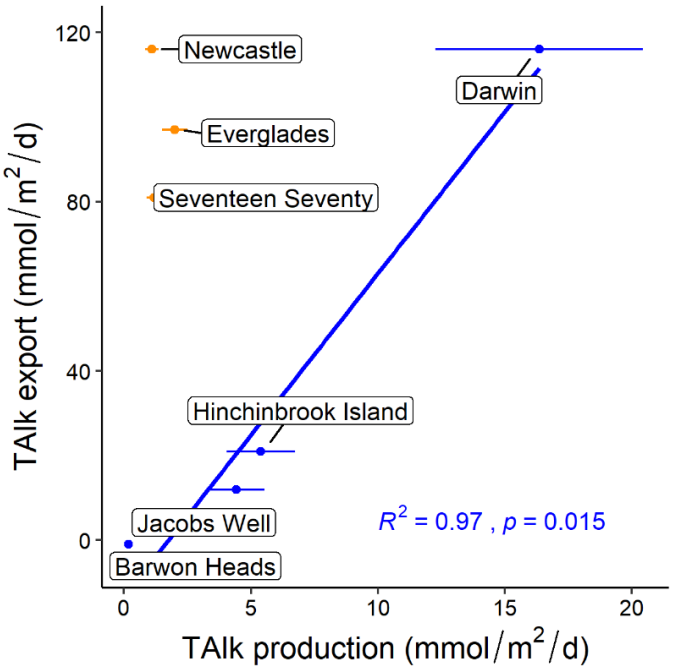

Figure 7. Mangrove TAlk export is plotted as a function of TAlk production coupled to pyrite formation. A linaer regression is shown for Barwon Heads, Jacobs Well, Hinchinbrook Isalnd and Darwin. Export values have been retrived from Reithmaier et al. (2020) (Everglades) and from Sippo et al. (2016) (remaining sites).

An important observation is that lateral TAlk export was ~ eight-fold higher than the estimated TAlk production coupled to pyrite formation (Figure 7). Firstly, this discrepancy might be a consequence of the contrasting time scales of TAlk production and export. Production of TAlk coupled to pyrite formation integrates several decades, whereas the measured TAlk export rates presented here for comparison were determined over two tidal cycles have been found to vary seasonally (Ho et al., 2017; Maher et al., 2013) and over spring-neap cycles (Taillardat et al., 2018), suggesting short-term measurements likely do not capture longer term rates. Secondly, the discrepancy might be due to additional TAlk production processes, such as denitrification, manganese reduction, iron reduction and carbonate dissolution (Krumins et al., 2013). It is also very likely, that a proportion of sulfate reduction is not coupled to pyrite formation (Berner, 1984), with some oxidation of exported reduced metabolites occurring outside of the mangroves, and therefore not accounted for in the lateral exchange method of Sippo et al. (2016). Consequently, future carbon sink estimates based on lateral TAlk exports should also assess export of reduced metabolites to provide a net estimate.

Sulfate reduction only contributes to net TAlk production if the reduced sulfur is spatially decoupled from bicarbonate ions and prevented from re-oxidising in a manner that consumes produced bicarbonate. In addition to pyrite formation, other processes can theoretically remove sulfide from mangrove sediments and result in pyrite being an underestimate of net TAlk production rates. For example, mangroves can remove reduced sulfur by assimilating and storing sulfide in their plant tissue (Fry et al., 1982; Okada & Sasaki, 1995). To the best of our knowledge, sulfide uptake rates by mangrove has not yet been quantified. Alongi et al. (2003) compiled mangrove tree sulfur content in *Avicenia marina* and *Rhizophera stylosa* stands and found an average of 0.6 and 2.1 Mg S/Ha, which, assuming all sulfur was associated with sulfide uptake, would only increase net TAlk production by between 0.4 and 11% for our sites.

In addition to plant uptake, reduced sulfur may be removed from the sediment by outgassing as hydrogen sulfide gas (H_2S) (Castro & Dierberg, 1987; Ganguly et al., 2018). There are limited forest-scale estimates of H_2S emissions. However, a study in the Sundarbans mangrove forest found emissions of 0.3 g S/m^2/y (Ganguly et al., 2018). If these emissions are representative of mangrove forests more generally, such gaseous H_2S flux would only result in a TAlk production (unaccounted for by pyrite) of 0.1 mmol/m^2/d an order of magnitude smaller than our pyrite-based estimates of TAlk production. Currently, sulfur removal by plant uptake and hydrogen sulfide emissions are not sufficiently quantified to constrain their effect on net TAlk production. However, this analysis suggests that their effect is likely to be minor compared to pyrite stocks.

Production and export of TAlk coupled to pyrite formation represent not only a blue carbon sink, but might also buffer coastal acidification (Sippo et al., 2016). Conversely, when pyrite is oxidised, net TAlk production can be reversed, resulting in acidity release that offsets blue carbon sinks. At Karumba, pyrite stocks were lower at the dead mangrove area compared to the living mangrove area, suggesting pyrite loss. At the living area, pyrite stocks were significantly correlated to groundwater TAlk, indicating that pyrite formation was linked to TAlk generation. Assuming similar pyrite concentrations in living and dead areas prior to the dieback, the dieback reversed the TAlk generation, releasing 54 mol/m^2 of acidity through the oxidation of pyrite. If pyrite was gradually lost over time, then 56 mmol/m^2/d of TAlk was lost as CO_2 emissions between the dieback and our sampling. This highlights that mangrove sediment disturbance leading to pyrite oxidation can reverse the TAlk carbon sink coupled to pyrite formation, releasing carbon to the atmosphere.

4.3 Global pyrite stocks and resulting alkalinity production in mangroves

From our data we constructed a global model for mangrove pyrite stocks and the associated TAlk production. Although sampling covered a broad range of climatic zones, it was limited to sites in Australia and the USA. Therefore, future research is encouraged to validate our model by quantifying pyrite stocks in other parts of the world, since to our knowledge no other mangrove pyrite stocks have been published. Despite the limitations of our model, it is a useful first order estimate to determine the general importance of alkalinity production coupled to pyrite formation on a global level.

Our model explained 78% of the variability in the observed mangrove pyrite stocks (Figure 8). The model data equation (-459.360057 – 2.348824 × Temperature (°C) + 0.176380 × Tidal amplitude (cm) + 89.656683 × ln(Sediment carbon stock (Mg/ha)) + 7.708681 × ln(Aboveground biomass (Mg/ha)) – 0.614195 × Latitude – 0.003740 × Rainfall (mm) + 35.784984 × ln(Catchment iron (mg/g)) is based on data presented in Table 3. By combining our model with published global datasets for key model parameters we estimate that

mangroves store in total 2.1 (25% to 75% percentile range of 1.8 – 2.5) Pg of pyrite globally to a depth of 1 m with an average of 155 (range = 128 – 182) Mg/ha (Figure 9).

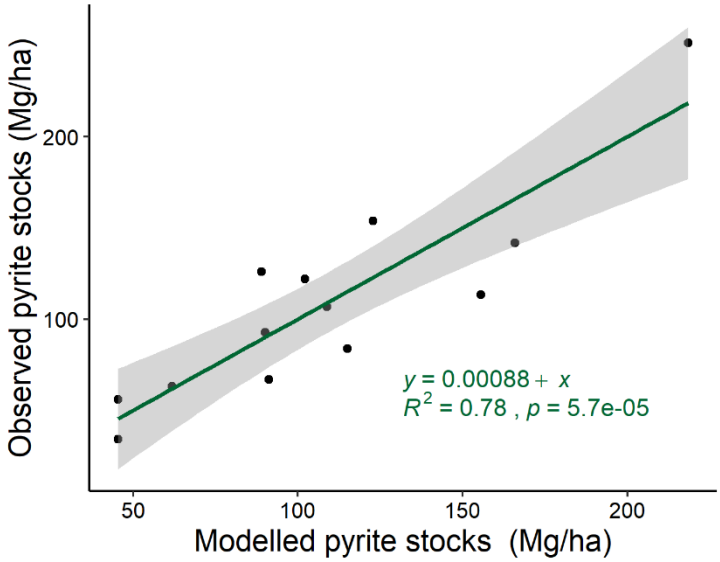

Figure 8. Correlation between observed and modelled mangrove pyrite stocks. The grey area shows the 95% confidence intervals of the regression. The regression has a slope of one.

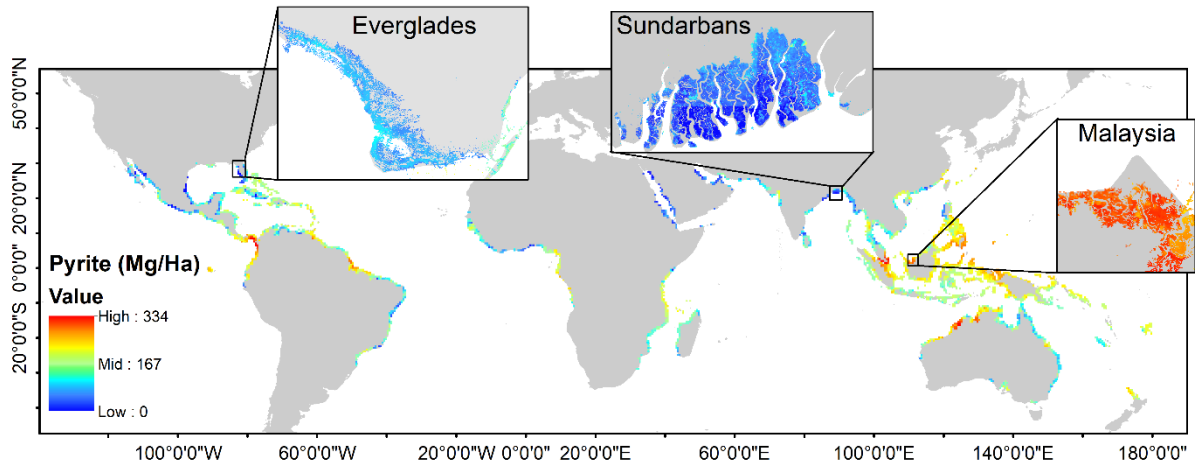

Figure 9. Global map of mangrove pyrite stocks and detailed maps of the Everglades, the Sundarbans and Malaysia.

Currently, no high-resolution global maps for SAR exist, therefore the TAlk production rate is limited to an empirical calculation. Multiplying the global average pyrite stocks by the global average SAR for mangroves (0.49 cm/y) determined by Alongi (2012), and converting it to TAlk production yields a total TAlk production that is coupled to global pyrite formation of 0.44 Tmol/y (range = 0.37 to 0.52 Tmol/y). This TAlk production rate is within the broad range estimated by Hu and Cai (2011), who used a range of sediment C/S ratios and carbon burial rates to estimate that pyrite formation in coastal vegetated habitats results in a net TAlk production of 0.1 – 1.1 Tmol/y. Our estimated global average TAlk production rate (3.2 mol/m^2/y, range = 2.7 – 3.8 mol/m^2/y), is equivalent to 24% (range = 19 – 27%) of the global organic carbon burial rate (14 mol/m^2/y) within mangrove sediments (Breithaupt et al., 2012), highlighting the importance of including this mode of TAlk generation into future blue carbon budgets.

Conclusion

The majority of blue carbon research has focused on organic carbon stocks, whereas TAlk production and export has been less investigated. Quantifying pyrite stocks and the associated TAlk production in coastal vegetated habitats, we found that alkalinity production coupled to pyrite formation might represent a significant blue carbon sink. However, the long-term production rates of pyrite are an order of magnitude smaller than short-term measured TAlk export rates, suggesting that the timescales of measurement, and methodology used need to be adequately addressed. While more research is required to understand the drivers and relevance of this process, we argue that pyrite accumulation should be included in the blue carbon paradigm as is represents a long-term carbon sink.

Acknowledgements

This research project was funded by the Australian Research Council (DP180101285). We would like to thank Roz Hagan for her support in the lab. Furthermore, we are grateful for generous support in the field to James Sippo, Julia Kalla, Yota Harada, Luke Jeffrey, Alice Gauthey, Geoff Balland, Sebastian Euler, Benjamin Hickman and James Ash. The authors declare that there is no conflict of interest. Datasets for this research have been submitted to the PANGAEA database. The data archiving is underway.

References

Alongi, D. M. (2012). Carbon sequestration in mangrove forests. *Carbon management*, *3*(3), 313-322.

Alongi, D. M., B. F. Clough, P. Dixon, & F. Tirendi (2003). Nutrient partitioning and storage in arid-zone forests of the mangroves Rhizophora stylosa and Avicenniamarina. *Trees*, *17*(1), 51-60.

Andrade, R., C. J. Sanders, G. Boaventura, & S. R. Patchineelam (2012). Pyritization of trace metals in mangrove sediments. *Environmental Earth Sciences*, *67*(6), 1757-1762. https://doi.org/10.1007/s12665-012-1620-4

APHA (2005). *Standard methods for the examination of water and wastewater*. Baltimore, MD: American Public Health Association – American Water Works Association.

Berner, R. A. (1970). Sedimentary pyrite formation. *American Journal of Science*, *268*(1), 1-23.

Berner, R. A. (1984). Sedimentary pyrite formation: an update. *Geochimica et Cosmochimica Acta*, *48*(4), 605-615. https://doi.org/10.1016/0016-7037(84)90089-9

Berner, R. A., & R. Raiswell (1984). C/S method for distinguishing freshwater from marine sedimentary rocks. *Geology*, *12*(6), 365-368. https://doi.org/10.1130/0091-7613(1984)12<365:CMFDFF>2.0.CO;2

Bianchi, T. S. (2007). *Biogeochemistry of estuaries*. New York, NY: Oxford University Press on Demand.

Blodau, C. (2006). A review of acidity generation and consumption in acidic coal mine lakes and their watersheds. *Science of the Total Environment*, *369*(1-3), 307-332. https://doi.org/10.1016/j.scitotenv.2006.05.004

Breithaupt, J. L., J. M. Smoak, T. J. Smith III, C. J. Sanders, & A. Hoare (2012). Organic carbon burial rates in mangrove sediments: Strengthening the global budget. *Global Biogeochemical Cycles*, *26*(3), GB3011. https://doi.org/10.1029/2012GB004375

Brown, D. R., S. Conrad, K. Akkerman, S. Fairfax, J. Fredericks, E. Hanrio, et al. (2016). Seagrass, mangrove and saltmarsh sedimentary carbon stocks in an urban estuary; Coffs Harbour, Australia. *Regional Studies in Marine Science*, *8*, 1-6. https://doi.org/10.1016/j.rsma.2016.08.005

Brown, M. I., T. Pearce, J. Leon, R. Sidle, & R. Wilson (2018). Using remote sensing and traditional ecological knowledge (TEK) to understand mangrove change on the Maroochy River, Queensland, Australia. *Applied Geography*, *94*, 71-83. https://doi.org/10.1016/j.apgeog.2018.03.006

Burdige, D. (2011). Estuarine and coastal sediments–coupled biogeochemical cycling. *Treatise on Estuarine and Coastal Science*, *5*, 279-308. https://doi.org/10.1002/2015GB005324

Bureau of Meteorology (2020). *Tide Tables*. Retrieved: 07/07/2020 from http://www.bom.gov.au/oceanography/projects/ntc/monthly/.

Burton, E. D., R. T. Bush, S. G. Johnston, L. A. Sullivan, & A. F. Keene (2011). Sulfur biogeochemical cycling and novel Fe–S mineralization pathways in a tidally re-flooded wetland. *Geochimica et Cosmochimica Acta*, *75*(12), 3434-3451. https://doi.org/10.1016/j.gca.2011.03.020

Burton, E. D., R. T. Bush, L. A. Sullivan, R. K. Hocking, D. R. Mitchell, S. G. Johnston, et al. (2009). Iron-monosulfide oxidation in natural sediments: resolving microbially mediated S transformations using XANES, electron microscopy, and selective extractions. *Environmental Science & Technology*, *43*(9), 3128-3134. https://doi.org/10.1021/es8036548

Burton, E. D., L. A. Sullivan, R. T. Bush, S. G. Johnston, & A. F. Keene (2008). A simple and inexpensive chromium-reducible sulfur method for acid-sulfate soils. *Applied Geochemistry*, *23*(9), 2759-2766. https://doi.org/10.1016/j.apgeochem.2008.07.007

Castro, M. S., & F. E. Dierberg (1987). Biogenic hydrogen sulfide emissions from selected Florida wetlands. *Water, Air, and Soil Pollution*, *33*(1-2), 1-13. https://doi.org/10.1007/BF00191372

Chanton, J. P., C. S. Martens, & M. B. Goldhaber (1987). Biogeochemical cycling in an organic-rich coastal marine basin. 8. A sulfur isotopic budget balanced by differential diffusion across the sediment-water interface. *Geochimica et Cosmochimica Acta*, *51*(5), 1201-1208. https://doi.org/10.1016/0016-7037(87)90212-2

Climate-Data.org (2020). *Climate data for cities worldwide*. Retrieved: 07/07/2020 from https://en.climate-data.org/.

Cline, J. D. (1969). Spectrophotometric determination of hydrogen sulfide in natural waters. *Limnology and Oceanography*, *14*(3), 454-458. https://doi.org/10.4319/lo.1969.14.3.0454

Conrad, S. R., I. R. Santos, D. R. Brown, L. M. Sanders, M. L. van Santen, & C. J. Sanders (2017). Mangrove sediments reveal records of development during the previous century (Coffs Creek estuary, Australia). *Marine Pollution Bulletin*, *122*(1-2), 441-445. https://doi.org/10.1016/j.marpolbul.2017.05.052

Crémière, A., H. Strauss, M. Sebilo, W.-L. Hong, O. Gros, S. Schmidt, et al. (2017). Sulfur diagenesis under rapid accumulation of organic-rich sediments in a marine mangrove from Guadeloupe (French West Indies). *Chemical Geology*, *454*, 67-79. https://doi.org/10.1016/j.chemgeo.2017.02.017

Dickson, A. G. (2010). Standards for ocean measurements. *Oceanography*, *23*(3), 34-47. https://doi.org/10.5670/oceanog.2010.22

Ding, H., S. Yao, & J. Chen (2014). Authigenic pyrite formation and re-oxidation as an indicator of an unsteady-state redox sedimentary environment: Evidence from the intertidal mangrove sediments of Hainan Island, China. *Continental Shelf Research*, *78*, 85-99. https://doi.org/10.1016/j.csr.2014.02.011

Donato, D. C., J. B. Kauffman, D. Murdiyarso, S. Kurnianto, M. Stidham, & M. Kanninen (2011). Mangroves among the most carbon-rich forests in the tropics. *Nature Geoscience*, *4*(5), 293. https://doi.org/10.1038/NGEO1123

Duke, N. C., J. M. Kovacs, A. D. Griffiths, L. Preece, D. J. Hill, P. Van Oosterzee, et al. (2017). Large-scale dieback of mangroves in Australia's Gulf of Carpentaria: a severe ecosystem response, coincidental with an unusually extreme weather event. *Marine and Freshwater Research*, *68*(10), 1816-1829. https://doi.org/10.1071/MF16322

Emerson, S., & J. Hedges (2008). *Chemical oceanography and the marine carbon cycle*. Cambridge, UK: Cambridge University Press. https://doi.org/10.1017/CBO9780511793202

Ferreira, T., X. Otero, P. Vidal-Torrado, & F. Macías (2007a). Effects of bioturbation by root and crab activity on iron and sulfur biogeochemistry in mangrove substrate. *Geoderma*, *142*(1-2), 36-46. https://doi.org/10.1016/j.geoderma.2007.07.010

Ferreira, T., X. Otero, P. Vidal-Torrado, & F. Macías (2007b). Redox processes in mangrove soils under Rhizophora mangle in relation to different environmental conditions. *Soil Science Society of America Journal*, *71*(2), 484-491. https://doi.org/10.2136/sssaj2006.0078

Fick, S. E., & R. J. Hijmans (2017). WorldClim 2: new 1-km spatial resolution climate surfaces for global land areas. *International Journal of Climatology*, *37*(12), 4302-4315. https://doi.org/10.1002/joc.5086

Fourqurean, J. W., C. M. Duarte, H. Kennedy, N. Marbà, M. Holmer, M. A. Mateo, et al. (2012). Seagrass ecosystems as a globally significant carbon stock. *Nature Geoscience*, *5*(7), 505-509. https://doi.org/10.1038/NGEO1477

Froelich, P. N., G. Klinkhammer, M. L. Bender, N. Luedtke, G. R. Heath, D. Cullen, et al. (1979). Early oxidation of organic matter in pelagic sediments of the eastern equatorial Atlantic: suboxic diagenesis. *Geochimica et Cosmochimica Acta*, *43*(7), 1075-1090.

Fry, B., R. S. Scalan, J. K. Winters, & P. L. Parker (1982). Sulphur uptake by salt grasses, mangroves, and seagrasses in anaerobic sediments. *Geochimica et Cosmochimica Acta*, *46*(6), 1121-1124. https://doi.org/10.1016/0016-7037(82)90063-1

Ganguly, D., R. Ray, N. Majumdar, C. Chowdhury, & T. Jana (2018). Biogenic hydrogen sulphide emissions and non-sea sulfate aerosols over the Indian Sundarban mangrove forest. *Journal of Atmospheric Chemistry*, *75*(3), 319-333. https://doi.org/10.1007/s10874-018-9382-3

Giblin, A. E. (1988). Pyrite formation in marshes during early diagenesis. *Geomicrobiology Journal*, *6*(2), 77-97. https://doi.org/10.1080/01490458809377827

Goldhaber, M. B. (2003). Sulfur-rich sediments. In F. T. Mackenzie, H. D. Holland and K. K. Turekian (Eds.), *Treatise on Geochemistry* (p. 407). Denver CO: US Geological Survey. https://doi.org/10.1016/B0-08-043751-6/07139-5

Hemond, H. F., W. K. Nuttle, R. W. Burke, & K. D. Stolzenbach (1984). Surface infiltration in salt marshes: Theory, measurement, and biogeochemical implications. *Water Resources Research*, *20*(5), 591-600. https://doi.org/10.1029/WR020i005p00591

Ho, D. T., S. Ferrón, V. C. Engel, W. T. Anderson, P. K. Swart, R. M. Price, & L. Barbero (2017). Dissolved carbon biogeochemistry and export in mangrove-dominated rivers of the Florida Everglades. *Biogeosciences*, *14*(9), 2543-2559. https://doi.org/10.5194/bg-14-2543-2017

Holmer, M., C. M. Duarte, & N. Marbá (2003). Sulfur cycling and seagrass (Posidonia oceanica) status in carbonate sediments. *Biogeochemistry*, *66*(3), 223-239. https://doi.org/10.1023/B:BIOG.0000005326.35071.51

Holmer, M., E. Kristensen, G. Banta, K. Hansen, M. H. Jensen, & N. Bussawarit (1994). Biogeochemical cycling of sulfur and iron in sediments of a south-east Asian mangrove, Phuket Island, Thailand. *Biogeochemistry*, *26*(3), 145-161. https://doi.org/10.1007/BF00002904

Holmer, M., O. Pedersen, & K. Ikejima (2006). Sulfur cycling and sulfide intrusion in mixed Southeast Asian tropical seagrass meadows. *Botanica Marina*, *49*(2), 91-102. https://doi.org/10.1515/BOT.2006.013

Howarth, R. W. (1979). Pyrite: its rapid formation in a salt marsh and its importance in ecosystem metabolism. *Science*, *203*(4375), 49-51. https://doi.org/10.1126/science.203.4375.49

Hu, X., & W. J. Cai (2011). An assessment of ocean margin anaerobic processes on oceanic alkalinity budget. *Global Biogeochemical Cycles*, *25*(3), GB3003. https://doi.org/10.1029/2010GB003859

Hutchison, J., A. Manica, R. Swetnam, A. Balmford, & M. Spalding (2014). Predicting global patterns in mangrove forest biomass. *Conservation Letters*, *7*(3), 233-240. https://doi.org/10.1111/conl.12060

Jeffrey, L. C., D. T. Maher, I. R. Santos, M. Call, M. J. Reading, C. Holloway, & D. R. Tait (2018). The spatial and temporal drivers of pCO_2, pCH_4 and gas transfer velocity within a subtropical estuary. *Estuarine, Coastal and Shelf Science*, *208*, 83-95. https://doi.org/10.1016/j.ecss.2018.04.022

Jerath, M., M. Bhat, V. H. Rivera-Monroy, E. Castañeda-Moya, M. Simard, & R. R. Twilley (2016). The role of economic, policy, and ecological factors in estimating the value of carbon stocks in Everglades mangrove forests, South Florida, USA. *Environmental Science & Policy*, *66*, 160-169. https://doi.org/10.1016/j.envsci.2016.09.005

Johnston, S. G., A. F. Keene, E. D. Burton, R. T. Bush, & L. A. Sullivan (2012). Quantifying alkalinity generating processes in a tidally remediating acidic wetland. *Chemical Geology*, *304*, 106-116. https://doi.org/10.1016/j.chemgeo.2012.02.008

Johnston, S. G., A. F. Keene, R. T. Bush, E. D. Burton, L. A. Sullivan, L. Isaacson, et al. (2011). Iron geochemical zonation in a tidally inundated acid sulfate soil wetland. *Chemical Geology*, *280*(3-4), 257-270. https://doi.org/10.1016/j.chemgeo.2010.11.014

Johnston, S. G., B. Morgan, & E. D. Burton (2016). Legacy impacts of acid sulfate soil runoff on mangrove sediments: Reactive iron accumulation, altered sulfur cycling and trace metal enrichment. *Chemical Geology*, *427*, 43-53. https://doi.org/10.1016/j.chemgeo.2016.02.013

Kauffman, J. B., & R. K. Bhomia (2017). Ecosystem carbon stocks of mangroves across broad environmental gradients in West-Central Africa: global and regional comparisons. *PloS ONE*, *12*(11), e0187749. https://doi.org/10.1371/journal.pone.0187749

Kelleway, J. J., N. Saintilan, P. I. Macreadie, & P. J. Ralph (2016). Sedimentary factors are key predictors of carbon storage in SE Australian saltmarshes. *Ecosystems*, *19*(5), 865-880. https://doi.org/10.1007/s10021-016-9972-3

Kendall, B., A. D. Anbar, A. Kappler, & K. O. Konhauser (2012). The global iron cycle. In A. H. Knoll, D. E. Canfield and K. O. Konhauser (Eds.), *Fundamentals of Geobiology* (pp. 65-92). West Sussex: Blackwell Publishing Ltd.

Komiyama, A., J. E. Ong, & S. Poungparn (2008). Allometry, biomass, and productivity of mangrove forests: A review. *Aquatic Botany*, *89*(2), 128-137. https://doi.org/10.1016/j.aquabot.2007.12.006

Kristensen, E., S. Bouillon, T. Dittmar, & C. Marchand (2008). Organic carbon dynamics in mangrove ecosystems: a review. *Aquatic Botany*, *89*(2), 201-219. https://doi.org/10.1016/j.aquabot.2007.12.005

Krumins, V., M. Gehlen, S. Arndt, P. V. Cappellen, & P. Regnier (2013). Dissolved inorganic carbon and alkalinity fluxes from coastal marine sediments: model estimates for different shelf environments and sensitivity to global change. *Biogeosciences*, *10*(1), 371-398. https://doi.org/10.5194/bg-10-371-2013

Lee, W., & D. Patterson (2002). Abundance and biomass of heterotrophic flagellates, and factors controlling their abundance and distribution in sediments of Botany Bay. *Microbial Ecology*, *43*, 467-481. https://doi.org/10.1007/s00248-002-2000-5

Logan, B., K. H. Taffs, B. D. Eyre, & A. Zawadski (2011). Assessing changes in nutrient status in the Richmond River estuary, Australia, using paleolimnological methods. *Journal of Paleolimnology*, *46*(4), 597-611. https://doi.org/10.1007/s10933-010-9457-x

Lovelock, C. E., I. C. Feller, R. Reef, S. Hickey, & M. C. Ball (2017). Mangrove dieback during fluctuating sea levels. *Scientific Reports*, *7*(1), 1680. https://doi.org/10.1038/s41598-017-01927-6

Luther III, G. W., A. Giblin, R. W. Howarth, & R. A. Ryans (1982). Pyrite and oxidized iron mineral phases formed from pyrite oxidation in salt marsh and estuarine sediments. *Geochimica et Cosmochimica Acta*, *46*(12), 2665-2669. https://doi.org/10.1016/0016-7037(82)90385-4

Machado, W., N. L. Borrelli, T. Ferreira, A. Marques, M. Osterrieth, & C. Guizan (2014). Trace metal pyritization variability in response to mangrove soil aerobic and anaerobic oxidation processes. *Marine Pollution Bulletin*, *79*(1-2), 365-370. https://doi.org//10.1016/j.marpolbul.2013.11.016

Macreadie, P., M. Baird, S. Trevathan-Tackett, A. Larkum, & P. Ralph (2014). Quantifying and modelling the carbon sequestration capacity of seagrass meadows – a critical assessment. *Marine Pollution Bulletin*, *83*(2), 430-439. https://doi.org/10.1016/j.marpolbul.2013.07.038

Macreadie, P. I., K. Allen, B. P. Kelaher, P. J. Ralph, & C. G. Skilbeck (2012). Paleoreconstruction of estuarine sediments reveal human-induced weakening of coastal carbon sinks. *Global Change Biology*, *18*(3), 891-901. https://doi.org/10.1111/j.1365-2486.2011.02582.x

Maher, D. T., M. Call, I. R. Santos, & C. J. Sanders (2018). Beyond burial: Lateral exchange is a significant atmospheric carbon sink in mangrove forests. *Biology Letters*, *14*(7), 20180200. https://doi.org/10.1098/rsbl.2018.0200

Maher, D. T., K. Cowley, I. R. Santos, P. Macklin, & B. D. Eyre (2015). Methane and carbon dioxide dynamics in a subtropical estuary over a diel cycle: Insights from automated in situ radioactive and stable isotope measurements. *Marine Chemistry*, *168*, 69-79. https://doi.org/10.1016/j.marchem.2014.10.017

Maher, D. T., I. R. Santos, L. Golsby-Smith, J. Gleeson, & B. D. Eyre (2013). Groundwater-derived dissolved inorganic and organic carbon exports from a mangrove tidal creek: The missing mangrove carbon sink? *Limnology and Oceanography*, *58*(2), 475-488. https://doi.org/10.4319/lo.2013.58.2.0475

Maher, D. T., J. Z. Sippo, D. R. Tait, C. Holloway, & I. R. Santos (2016). Pristine mangrove creek waters are a sink of nitrous oxide. *Scientific Reports*, *6*, 25701. https://doi.org/10.1038/srep25701

Mcleod, E., G. L. Chmura, S. Bouillon, R. Salm, M. Björk, C. M. Duarte, et al. (2011). A blueprint for blue carbon: toward an improved understanding of the role of vegetated coastal habitats in sequestering CO_2. *Frontiers in Ecology and the Environment*, *9*(10), 552-560. https://doi.org/10.1890/110004

Middelburg, J. J., K. Soetaert, & M. Hagens (2019). Ocean alkalinity, buffering and biogeochemical processes. *Reviews of Geophysics*, e2019RG000681.

Millero, F. J., K. Lee, & M. Roche (1998). Distribution of alkalinity in the surface waters of the major oceans. *Marine Chemistry*, *60*(1-2), 111-130. https://doi.org/10.1016/S0304-4203(97)00084-4

Morse, J. W. (1999). Sulfides in sandy sediments: new insights on the reactions responsible for sedimentary pyrite formation. *Aquatic Geochemistry*, *5*(1), 75-85. https://doi.org/10.1023/A:1009620021442

Morse, J. W., H. Thomson, & D. W. Finneran (2007). Factors controlling sulfide geochemistry in sub-tropical estuarine and bay sediments. *Aquatic Geochemistry*, *13*(2), 143-156. https://doi.org/10.1007/s10498-007-9012-1

Nellemann, C., & E. Corcoran (2009). *Blue carbon: the role of healthy oceans in binding carbon: a rapid response assessment*. Birkeland, Norway: UNEP/Earthprint.

Okada, N., & A. Sasaki (1995). Characteristics of Sulfur Uptake by Mangroves: an Isotopic Study. *Tropics*, *4*(2+3), 201-210. https://doi.org/10.3759/tropics.4.201

Otero, X., T. Ferreira, M. Huerta-Díaz, C. S. d. M. Partiti, V. Souza Jr, P. Vidal-Torrado, & F. Macías (2009). Geochemistry of iron and manganese in soils and sediments of a mangrove system, Island of Pai Matos (Cananeia - SP, Brazil). *Geoderma*, *148*(3-4), 318-335. https://doi.org/10.1016/j.geoderma.2008.10.016

Ouyang, X., & S. Lee (2014). Updated estimates of carbon accumulation rates in coastal marsh sediments. *Biogeosciences*, 5057. https://doi.org/10.5194/bg-11-5057-2014

Radabaugh, K. R., R. P. Moyer, A. R. Chappel, C. E. Powell, I. Bociu, B. C. Clark, & J. M. Smoak (2018). Coastal blue carbon assessment of mangroves, salt marshes, and salt barrens in Tampa Bay, Florida, USA. *Estuaries and Coasts*, *41*(5), 1496-1510. https://doi.org/10.1007/s12237-017-0362-7

Raiswell, R., D. Canfield, & R. Berner (1994). A comparison of iron extraction methods for the determination of degree of pyritisation and the recognition of iron-limited pyrite formation. *Chemical Geology*, *111*(1-4), 101-110. https://doi.org/10.1016/0009-2541(94)90084-1

Raiswell, R., & D. E. Canfield (2012). The iron biogeochemical cycle past and present. *Geochemical perspectives*, *1*(1), 1-2.

Reithmaier, G., D. T. Ho, S. Johnston, & D. Maher (2020), Mangroves as a Source of Alkalinity and Dissolved Carbon to the Coastal Ocean: A Case Study from the Everglades National Park, Florida. Dataset edited and distributed by PANGAEA. https://doi.org/10.1594/PANGAEA.916154

Rickard, D. (1997). Kinetics of pyrite formation by the H_2S oxidation of iron (II) monosulfide in aqueous solutions between 25 and 125 C: the rate equation. *Geochimica et Cosmochimica Acta*, *61*(1), 115-134. https://doi.org/10.1016/S0016-7037(96)00321-3

Rickard, D., & G. W. Luther (2007). Chemistry of iron sulfides. *Chemical Reviews*, *107*(2), 514-562. https://doi.org/10.1021/cr0503658

Robador, A., A. L. Müller, J. E. Sawicka, D. Berry, C. R. Hubert, A. Loy, et al. (2016). Activity and community structures of sulfate-reducing microorganisms in polar, temperate and tropical marine sediments. *The ISME journal*, *10*(4), 796-809. https://doi.org/10.1038/ismej.2015.157

Rossel, R. V., T. Behrens, E. Ben-Dor, D. Brown, J. Demattê, K. D. Shepherd, et al. (2016). A global spectral library to characterize the world's soil. *Earth-Science Reviews*, *155*, 198-230. https://doi.org/10.1016/j.earscirev.2016.01.012

Sadat-Noori, M., I. R. Santos, D. R. Tait, M. J. Reading, & C. J. Sanders (2017). High porewater exchange in a mangrove-dominated estuary revealed from short-lived radium isotopes. *Journal of Hydrology*, *553*, 188-198. https://doi.org/10.1016/j.jhydrol.2017.07.058

Sanderman, J., T. Hengl, G. Fiske, K. Solvik, M. F. Adame, L. Benson, et al. (2018). A global map of mangrove forest soil carbon at 30 m spatial resolution. *Environmental Research Letters*, *13*(5), 055002. https://doi.org/10.1088/1748-9326/aabe1c

Sanders, C. J., D. T. Maher, D. R. Tait, D. Williams, C. Holloway, J. Z. Sippo, & I. R. Santos (2016a). Are global mangrove carbon stocks driven by rainfall? *Journal of Geophysical Research: Biogeosciences*, *121*(10), 2600-2609. https://doi.org/10.1002/2016JG003510.

Sanders, C. J., I. R. Santos, D. T. Maher, J. L. Breithaupt, J. M. Smoak, M. Ketterer, et al. (2016b). Examining $^{239+240}Pu$, ^{210}Pb and historical events to determine carbon, nitrogen and phosphorus burial in mangrove sediments of Moreton Bay, Australia. *Journal of Environmental Radioactivity*, *151*, 623-629. https://doi.org/10.1016/j.jenvrad.2015.04.018

Santos, I. R., D. T. Maher, R. Larkin, J. R. Webb, & C. J. Sanders (2019). Carbon outwelling and outgassing vs. burial in an estuarine tidal creek surrounded by mangrove and saltmarsh wetlands. *Limnology and Oceanography*, *64*(3), 996-1013. https://doi.org/10.1002/lno.11090

Sasmito, S. D., M. Sillanpää, M. A. Hayes, S. Bachri, M. F. Saragi-Sasmito, F. Sidik, et al. (2020). Mangrove blue carbon stocks and dynamics are controlled by hydrogeomorphic settings and land-use change. *Global Change Biology*, *26*(5), 3028-3039. https://doi.org/10.1111/gcb.15056

Schoonen, M., & H. Barnes (1991). Reactions forming pyrite and marcasite from solution: II. Via FeS precursors below 100 C. *Geochimica et Cosmochimica Acta*, *55*(6), 1505-1514. https://doi.org/10.1016/0016-7037(91)90123-M

Sheoran, A., V. Sheoran, & R. Choudhary (2010). Bioremediation of acid-rock drainage by sulphate-reducing prokaryotes: a review. *Minerals Engineering*, *23*(14), 1073-1100. https://doi.org/10.1016/j.mineng.2010.07.001

Sherman, R. E., T. J. Fahey, & R. W. Howarth (1998). Soil-plant interactions in a neotropical mangrove forest: iron, phosphorus and sulfur dynamics. *Oecologia*, *115*(4), 553-563. https://doi.org/10.1007/s004420050553

Simard, M., T. Fatoyinbof, C. Smetankas, V. Rivera-Monroy, E. Castaneda-Mova, N. Thomas, & T. Van der Stocken (2019). *Global Mangrove Distribution, Aboveground Biomass, and Canopy Height*. Oak Ridge, TN: ORNL DAAC. https://doi.org/10.3334/ORNLDAAC/1665

Sippo, J. Z., D. T. Maher, D. R. Tait, C. Holloway, & I. R. Santos (2016). Are mangroves drivers or buffers of coastal acidification? Insights from alkalinity and dissolved inorganic carbon export estimates across a latitudinal transect. *Global Biogeochemical Cycles*, *30*(5), 753-766. https://doi.org/10.1002/2015gb005324

Sippo, J. Z., C. J. Sanders, I. R. Santos, L. C. Jeffrey, M. Call, Y. Harada, et al. (2020). Coastal carbon cycle changes following mangrove loss. *Limnol. Oceanogr*, *9999*, 1-15. https://doi.org/10.1002/lno.11476

Smoak, J. M., J. L. Breithaupt, T. J. Smith III, & C. J. Sanders (2013). Sediment accretion and organic carbon burial relative to sea-level rise and storm events in two mangrove forests in Everglades National Park. *Catena*, *104*, 58-66. https://doi.org/10.1016/j.catena.2012.10.009

Taillardat, P., P. Willemsen, C. Marchand, D. Friess, D. Widory, P. Baudron, et al. (2018). Assessing the contribution of porewater discharge in carbon export and CO_2 evasion in a mangrove tidal creek (Can Gio, Vietnam). *Journal of Hydrology*, *563*, 303-318. https://doi.org/10.1016/j.jhydrol.2018.05.042

Tait, D. R., D. T. Maher, P. A. Macklin, & I. R. Santos (2016). Mangrove pore water exchange across a latitudinal gradient. *Geophysical Research Letters*, *43*(7), 3334-3341. https://doi.org/10.1002/2016GL068289

Vestbo, S., M. Obst, F. J. Quevedo Fernandez, I. Intanai, & P. Funch (2018). Present and potential future distributions of asian horseshoe crabs determine areas for conservation. *Frontiers in Marine Science*, *5*, 164. https://doi.org/10.3389/fmars.2018.00164

Wada, H., & B. Seisuwan (1986). *The process of pyrite formation in mangrove soils*. Paper presented at Third International Symposium on Acid Sulphate Soil, Dakar, Senegal.

Wang, Z. A., & W. J. Cai (2004). Carbon dioxide degassing and inorganic carbon export from a marsh-dominated estuary (the Duplin River): A marsh CO_2 pump. *Limnology and Oceanography*, *49*(2), 341-354. https://doi.org/10.4319/lo.2004.49.2.0341

Westrich, J. T., & R. A. Berner (1988). The effect of temperature on rates of sulfate reduction in marine sediments. *Geomicrobiology Journal*, *6*(2), 99-117. https://doi.org/10.1080/01490458809377828